

Shape of solar cycles and mid-term solar activity oscillations

D. Sokoloff^{1,2,3*}, A.S. Shibalova^{2,†}, V.N. Obridko^{2,‡}, V. Pipin^{4,§}

¹*Department of Physics, Moscow State University, Moscow, 119992, Russia*

²*IZMIRAN, 4 Kaluzhskoe Shosse, Troitsk, Moscow, 142190*

³*Moscow Center of Fundamental and Applied Mathematics, Moscow, 119991, Russia*

⁴*Institute of Solar-Terrestrial Physics, Russian Academy of Sciences, Irkutsk, 664033, Russia*

4 August 2020

ABSTRACT

The evolution of the solar activity comprises, apart from the well-known 11-year cycle, various temporal scales ranging from months up to the secondary cycles known as mid-term oscillations. Its nature deserves a physical explanation. In this work, we have considered the 5-to-6 year oscillations as derived both from sunspot and from solar magnetic dipole time series. Using solar dynamo model, we have deduced that these variations may be a manifestation of the dynamo nonlinearities and non-harmonic shape of the solar activity cycles. We have concluded that the observed mid-term oscillations are related to the nonlinear saturation of the dynamo processes in the solar interior.

Key words: Sun: magnetic fields; Sun: oscillations; sunspots

1 INTRODUCTION

The most pronounced feature in the time evolution of the solar activity is the well-known 11-year sunspot cycle with the 22-year oscillations of the solar magnetic field polarity underlying it. The evolution comprises also various shorter temporal scales known as mid-term oscillations (MTO) that range from months up to several years. The best known MTO are the so-called quasi-biennial oscillations, QBO (see, for example, the comprehensive review by Bazilevskaya et al. (2014) and references therein). The periodicities in this range are sometimes referred to as intermediate- or mid-term quasi-periodicities (e.g., Lou et al. (2003)). Another mid-term periodicity that was reported is the six-year oscillations Prabhakaran Nayar et al. (2002). For this phenomenon, we propose the term Quasi-Sexennial Oscillations (QSO). These two components of MTO (QBO and QSO) have different properties, and perhaps, different origins.

In this paper, we concentrate mainly on the analysis of QSO. Experimental data on QSO are rather scarce. This is because the periods of 4-6 years are difficult to isolate from the full spectrum in the vicinity of a powerful 11-year spectral peak. One way to improve the reliability of the detection of QSO parameters is to use a time series that has at least 100 years of data. The sunspot number record has one of the longest available time series of the solar activity tracers. The results of Frick et al. (2020) show that mid-term oscillations

(including QBO and QSO) in the sunspot numbers can be considered elements of the continuous spectrum typical of various turbulent or convective systems. Nevertheless, some features and characteristics of this spectrum can be originated in a deterministic way, e.g., due to nonlinearities in the large-scale dynamos.

According to Parker (1955), the solar dynamo involves two major components of the magnetic activity. The large-scale toroidal field produces bipolar regions, which emerge in the form of sunspots, and the large-scale poloidal field forms the shape of the solar corona. Correspondingly, we consider QSO both in sunspot tracers and in the tracers of the global magnetic field observed on the solar surface. Based on a joint analysis of the sunspot number, properties of the solar-wind plasma, interplanetary magnetic field, and geomagnetic activity index A_p , Prabhakaran Nayar et al. (2002) found variations with periods of about 5.5 years. Deng et al. (2014) identified variations with a period of 4-5 years while analyzing the characteristics of polar plages. Oscillations in the QSO range were later re-discovered by Deng et al. (2020) from data on the solar corona rotation over 80 years. Early on, Rivin & Obridko (1992) found variations with a period of about 6 years by analyzing the spectrum of the magnetic field of the Sun as a star based on the data of the John Wilcox Observatory in Stanford. Livshits & Obridko (2006) studied separately the cyclic variations of the axial and equatorial dipoles of the Sun. They found out that 5-year variations were observed only in the axial dipole record.

In search for an explanation of the MTO phenomenon, we recall that the continuous turbulent spectrum in the Kolmogorov turbulence is connected with the presence of the

* email: sokoloff.dd@gmail.com

† email: as.shibalova@physics.msu.ru

‡ email: obridko@izmiran.ru

§ email: pip@iszf.irk.ru

nonlinear transport term $\mathbf{v} \cdot \nabla \mathbf{v}$ in the Navier-Stokes equation. Because of this term, a large vortex of scale l produces two vortices of a smaller scale $l/2$, while the vortex wave vector k produces the wave vector $2k$. This is a standard explanation for the nature of the turbulent cascade. This explanation is, however, not immediately applicable to the case under discussion. Moreover, the proper oscillation scale for the magnetic field is 22 years, while 11 years is only the oscillation scale for the magnetic energy.

On the other hand, quadratic terms are present in such a problem. For example, the magnetic force acting on the flows and affecting the dynamo efficiency is quadratic with respect to the magnetic field. Also, the five years variation is, indeed, about half the duration of the 11-yr solar cycle. It seems plausible that something similar to a turbulent cascade may take place in the solar activity engine. Of course, this analogy is a very rough hint but most certainly worthy of a proper investigation here. This is the aim of our paper.

2 OBSERVATIONAL BASIS

In the present work, we are using the sunspot numbers and the parameters of the dipole term in the multipole expansion of the surface large-scale magnetic field as observational characteristics of the solar activity variations.

The raw monthly mean sunspot numbers SSN were borrowed from WDC-SILSO summary data, Royal Observatory of Belgium, Brussels (<http://sidc.oma.be/silso/datafiles>, version 2)

Using the Wilcox Solar Observatory (WSO) synoptic charts of the radial component of the solar magnetic field [Scherrer et al. \(1977\)](#), we calculated the magnetic field under the potential approximation by the well-known method described in [Hoeksema & Scherrer \(1986\)](#) and [Hoeksema \(1991\)](#). The method was applied in its classical version, without assuming radial field in the photosphere. WSO measurements of the magnetic-field longitudinal component were used as the source data to plot the synoptic charts for each Carrington rotation. The WSO data used in this study cover a time interval of 43 years from the beginning of Carrington rotation (CR) 1642 (27 May 1976) to the end of CR 2210 (November 2018).

The magnetic field parameters were calculated by solving the boundary-value problem for the line-of-sight field component measured in the photosphere and a strictly radial field at the source surface. The latter is assumed to be located at a distance of 2.5 radii from the center of the Sun.

The results are expressed in terms of the expansion in the Legendre polynomials. The terms g_{lm} and h_{lm} are the coefficients of the spherical harmonic analysis obtained by comparison with observations at the photospheric level. It is important to note that the coefficients were calculated under the assumption that the field is potential throughout the photosphere up to the source surface, including the boundaries. These coefficients determine the contribution of various multipoles and their direction. The dipole magnetic moment M_{dip} , the axial dipole moment M_{ax} , and the equatorial dipole moment M_{eq} are determined by the following

equations:

$$M_{\text{dip}} = \sqrt{g_{10}^2 + g_{11}^2 + h_{11}^2}, \quad (1)$$

$$M_{\text{ax}} = |g_{10}|, \quad M_{\text{eq}} = \sqrt{g_{11}^2 + h_{11}^2}. \quad (2)$$

As a first step in this paper, we will discuss variations in the solar dipole, since it is most simply related to the main mechanism of generation of the magnetic field. It is easy to model and its oscillations have the simplest form. Despite its simplicity, the dipole demonstrates the main features characteristic of the general description of solar activity: the solar dipole magnetic field displays both axisymmetric and non-axisymmetric components, whose variations with latitude and phase of the cycle obey the basic laws of solar activity as a whole.

3 THE SEARCH FOR MTO USING WAVELET ANALYSIS

The Fourier analysis is a traditional way to search for periodicity in stationary, strictly periodic or localized signals. The wavelet analysis has been applied to take into account quasi-periodic processes and time-localized periodicities (see e.g., [Frick et al. \(2020\)](#) in the context of solar activity problems). This method compares the signal with localized waves unlike the harmonic decomposition with an infinite sinusoidal signal. The wavelet existence time depends on two parameters - the wave position t and the characteristic scale a .

The general wavelet transform of function $f(t)$ is defined as

$$W(a, t) = C_{\psi}^{-1/2} a^{-1/2} \int_{-\infty}^{\infty} \psi^* \left(\frac{t' - t}{a} \right) f(t') dt', \quad (3)$$

where $\psi(t)$ means the basic wavelet function, $*$ denotes a complex conjugation, and coefficient C_{ψ} is determined through a Fourier transform of the basic wavelet $\hat{\psi}(\omega)$:

$$C_{\psi} = \int_{-\infty}^{\infty} |\omega|^{-1} |\hat{\psi}(\omega)|^2 d\omega. \quad (4)$$

The most widely used wavelets are derivatives of the Gaussian function. In our paper, we consider one of them — a complex valued Morlet wavelet

$$\psi(t) = e^{-t^2/\alpha^2} e^{i\omega t}, \quad (5)$$

with the parameters $\alpha^2 = 2$ and $\omega = 2\pi$.

The global wavelet spectrum

$$S(a) = \int |W(a, t)|^2 dt \quad (6)$$

shows the scale distribution of energy.

The reliability of the wavelet analysis depends on the length of the data record. It is usually sufficient if the realization is at least three times longer than the expected oscillation period. In our case, the length of the magnetic-field database (43 years) ensures the reliability of the detected periods no longer than 11-15 years. Therefore, the results obtained here for Mid-Term Oscillations (MTO) are quite reliable. Furthermore, the sunspot data we are using cover a period of more than 200 years. Therefore, the given sets of data are sufficient to reliably characterize the MTO parameters.

4 DYNAMO MODEL

In this paper, we are using the dynamo model proposed by Pipin & Kosovichev (2018b). It includes the minimal set of the dynamo equations to model the evolution of the non-axisymmetric magnetic field. Similarly to Moss et al. (2008), we neglect the radial dependence of the magnetic field and assume that the radial gradient of the angular velocity is larger than the latitudinal gradient. The evolution of the large-scale magnetic field induction vector $\langle \mathbf{B} \rangle$ in a perfectly conductive medium is governed by the mean-field equation

$$\partial_t \langle \mathbf{B} \rangle = \nabla \times (\mathcal{E} + \langle \mathbf{U} \rangle \times \langle \mathbf{B} \rangle), \quad (7)$$

where, $\mathcal{E} = \langle \mathbf{u} \times \mathbf{b} \rangle$ is the mean electromotive force with \mathbf{u} and \mathbf{b} standing for the turbulent velocity and magnetic field, respectively. It is convenient to represent the vector $\langle \mathbf{B} \rangle$ in terms of the axisymmetric and non-axisymmetric components as follows:

$$\langle \mathbf{B} \rangle = \bar{\mathbf{B}} + \tilde{\mathbf{B}} \quad (8)$$

$$\bar{\mathbf{B}} = \hat{\phi} B + \nabla \times (A \hat{\phi}) \quad (9)$$

$$\tilde{\mathbf{B}} = \nabla \times (\mathbf{r}T) + \nabla \times \nabla \times (\mathbf{r}S), \quad (10)$$

where $\bar{\mathbf{B}}$ and $\tilde{\mathbf{B}}$ are the axisymmetric and non-axisymmetric components; A , B , T , and S are the scalar functions representing the field components; $\hat{\phi}$ is the azimuthal unit vector, \mathbf{r} is the radius vector; r is the radial distance, and θ is the polar angle. Hereafter, the overbar denotes the axisymmetric magnetic field, and the tilde denotes non-axisymmetric properties.

Following the ideas outlined above, we now consider a reduced dynamo model where we neglect the radial dependence of the magnetic field. In this case, the induction vector of the large-scale magnetic field is represented in terms of the scalar functions as follows:

$$\langle \mathbf{B} \rangle = -\frac{\mathbf{r}}{R^2} \frac{\partial \sin \theta A}{\partial \mu} - \frac{\hat{\theta}}{R} A + \hat{\phi} B \quad (11)$$

$$- \frac{\mathbf{r}}{R^2} \Delta_\Omega S + \frac{\hat{\theta}}{\sin \theta} \frac{\partial T}{\partial \phi} + \hat{\phi} \sin \theta \frac{\partial T}{\partial \mu},$$

where R represents the radius of the spherical surface inside a star where the hydromagnetic dynamo operates. The above equation defines the 3d divergence-free B-field on the sphere. The model employs the following expression for \mathcal{E} :

$$\mathcal{E} = \alpha \langle \mathbf{B} \rangle - \eta_T \nabla \times \langle \mathbf{B} \rangle + V_\beta \hat{\mathbf{r}} \times \mathbf{B}. \quad (12)$$

Applying these simplifications to Eq (7) and Eqs (8-10), we obtain the following set of dynamo equations in terms of the scalar functions, A , B , S , and T :

$$\partial_t B = -\sin \theta \frac{\partial \Omega}{\partial r} \frac{\partial (\sin \theta A)}{\partial \mu} + \eta_T \frac{\sin^2 \theta}{R^2} \frac{\partial^2 (\sin \theta B)}{\partial \mu^2} \quad (13)$$

$$+ \frac{\sin \theta}{R} \frac{\partial}{\partial \mu} \alpha_0 \mu \langle B_r \rangle + \frac{\alpha_0 \mu}{R} \langle B_\theta \rangle$$

$$- \frac{1}{R} V_\beta \langle B_\phi \rangle - \frac{B}{\tau}$$

$$\partial_t A = \alpha_0 \mu \langle B_\phi \rangle + \eta_T \frac{\sin^2 \theta}{R^2} \frac{\partial^2 (\sin \theta A)}{\partial \mu^2} - \frac{V_\beta}{R} A - \frac{A}{\tau}, \quad (14)$$

To obtain the evolution equations for potential S and T , we

follow the procedure described in detail in Krause & Rädler (1980). We get,

$$\partial_t \Delta_\Omega T = -\Delta_\Omega \delta \Omega \frac{\partial T}{\partial \phi} + \frac{\eta_T}{R^2} \Delta_\Omega^2 T \quad (15)$$

$$- \frac{1}{R} \frac{\partial \Omega}{\partial r} \sin^2 \theta \frac{\partial \Delta_\Omega S}{\partial \mu} - \frac{1}{R} \frac{\partial}{\partial \phi} \left[\frac{\alpha_0}{\sin \theta} \mu \langle B_\phi \rangle \right]$$

$$+ \Delta_\Omega \frac{\alpha_0 \mu}{R} (\langle B_r \rangle \sin^2 \theta + \mu \sin \theta \langle B_\theta \rangle)$$

$$+ \frac{1}{R} \frac{\partial}{\partial \mu} \alpha_0 \mu \sin \theta \{ \mu \sin \theta \langle B_r \rangle + \mu^2 \langle B_\theta \rangle \}$$

$$- \frac{1}{R \sin \theta} \frac{\partial}{\partial \phi} \langle B_\theta \rangle V_\beta - \frac{\partial}{\partial \mu} (\sin \theta \langle B_\phi \rangle V_\beta),$$

$$\partial_t \Delta_\Omega S = -\left(\delta \Omega \Delta_\Omega \frac{\partial S}{\partial \phi} \right) + \frac{\eta_T}{R^2} \Delta_\Omega^2 S \quad (16)$$

$$+ \frac{\partial}{\partial \mu} \alpha_0 \mu \sin \theta \langle B_\phi \rangle$$

$$+ \frac{\partial}{\partial \phi} \left\{ \frac{\alpha_0 \mu}{\sin \theta} (\langle B_\theta \rangle + \sin \theta (\mathbf{e} \cdot \langle \mathbf{B} \rangle)) \right\}$$

$$- \frac{1}{\sin \theta} \frac{\partial}{\partial \phi} (\langle B_\phi \rangle V_\beta) + \frac{\partial}{\partial \mu} (\sin \theta \langle B_\theta \rangle V_\beta),$$

where $\Delta_\Omega = \frac{\partial}{\partial \mu} \sin^2 \theta \frac{\partial}{\partial \mu} + \frac{1}{\sin^2 \theta} \frac{\partial^2}{\partial \phi^2}$ and $\mu = \cos \theta$. To simulate the stretching of non-axisymmetric magnetic field by the surface differential rotation, we consider the latitudinal dependence of the angular velocity $\delta \Omega = -0.25 \sin^2 \theta \Omega$ in Eqs (15) and (16), which are written in the coordinate system rotating with angular velocity Ω . The τ -terms in Eqs(13,14) were suggested by Moss et al. (2008) to account for turbulent diffusion in the radial direction. Similarly to the cited paper, we put $\tau = 3 \frac{R^2}{\eta_T}$. The magnetic buoyancy is the source of the non-axisymmetric magnetic field in the model. We assume that the magnetic buoyancy affects relatively small-scale parts of the axisymmetric magnetic field, perhaps, because of some kind of nonlinear instability, and contributes to the induction of the non-axisymmetric magnetic field component. In the mean-field models, the magnetic buoyancy acts to produce a nonlinear turbulent pumping effect. Following Kitchatinov & Pipin (1993), we have:

$$V_\beta = \begin{cases} \frac{\alpha_{MLT} u'}{\gamma} \beta^2 K(\beta) [1 + \xi_\beta(\phi)], & \text{if } \beta \geq \beta_{cr}, \\ 0, & \text{if } \beta < \beta_{cr} \end{cases} \quad (17)$$

where $\beta = |\langle \mathbf{B} \rangle| / B_{\text{eq}}$, $B_{\text{eq}} = \sqrt{4\pi \rho u'^2}$, function $K(\beta)$ is defined in Kitchatinov & Pipin (1993), function $\xi_\beta(\phi)$ describes the longitudinal dependence of the instability, and parameter β_{cr} controls the instability threshold. These parameters will be described below. As follows from the paper cited above, for $\beta \ll 1$, $K(\beta) \sim 1$, and for $\beta > 1$, $K(\beta) \sim 1/\beta^3$. In this formulation, the preferable latitude of the ‘‘active region emergence’’ is determined by the maximum energy of the toroidal magnetic field, see Eq.(17). Parameter $\beta_{cr} = 0.5$ is adopted to prevent the emergence of active regions at high latitudes. For further details concerning the model see Pipin & Kosovichev (2018b). Also, the python code for the model can be found in Pipin (2020). Fig. 1 shows snapshots of the radial magnetic field in the model during the maxima and minima of the dynamo cycle. More details about the model can be found in Pipin & Kosovichev (2018a).

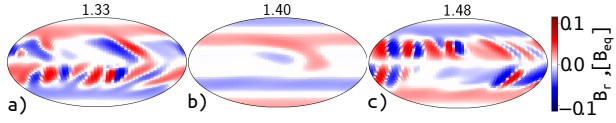


Figure 1. Snapshots of the radial distribution of the magnetic field in the model for the cycle maximum (a) and (c) and for the cycle minimum (b). The time above the snapshots is given in diffusive units.

Note that the magnetic buoyancy is the only nonlinear effect in the model. Therefore, the magnetic flux loss determines the amplitude of the dynamo waves. The lower the parameter β_{cr} , the more efficient the magnetic flux loss and the smaller the magnitude of the large-scale toroidal magnetic field. The time in the model is measured in diffusive units. Here, we scale the dynamo period to be about 10 years.

5 RESULTS: QSO IN SUNSPOT DATA AND IN SOLAR MAGNETOGRAMS

In this section, we discuss the QSO manifestations in the observational parameters. Then, we compare the observations with the results obtained from our solar dynamo model.

We start with a straightforward search for QSO in the Fourier spectra for sunspot data. Fig. 2a presents the integral Fourier spectrum for the monthly mean sunspot data from 1749 up to 2019. As expected, the peak corresponding to the Schwabe cycle is dominant in the plot. However, the point is that an additional peak near 6 years is visible, as well.

Fig. 2b shows the integral wavelet spectra for the sunspot time series from 1749 up to 2019 (middle panel). Apart from the expected 11-year peak, we recognize a much smaller peak at about 5 years. The wavelet plane (Fig. 2c) shows the long-term evolution of the sunspot number QSO. One can see that QSOs have a considerable magnitude only during the epochs of the centennial maxima. Below, we show how this phenomenon can be explained in terms of the nonlinear dynamo model.

From the viewpoint of the solar dynamo, the sunspot data trace the solar toroidal magnetic field. The poloidal magnetic field is another component of the large-scale solar activity. The axial magnetic dipole is a proxy parameter, which measures the strength and direction of the large-scale poloidal magnetic field. We employ the strength of the equatorial dipole as a proxy for the sunspot activity. Fig. 3 (top) shows the integral wavelet spectrum for the solar magnetic dipole. Since the magnetic dipole has two components of substantially different nature, i.e., the axial and the equatorial dipoles, their corresponding spectra are given separately.

A comparison of Fig. 2b and Fig. 3a shows that QSOs with a period of 5 years are better pronounced on the plot for the axial dipole than in the sunspot data. In contrast, the peak is absent in the integral wavelet spectrum for the equatorial dipole (see Fig. 3a). This empirical result sounds reasonable from the theoretical point of view, because it is the solar toroidal magnetic field and the axisymmetric part of the solar poloidal magnetic field that are involved in the

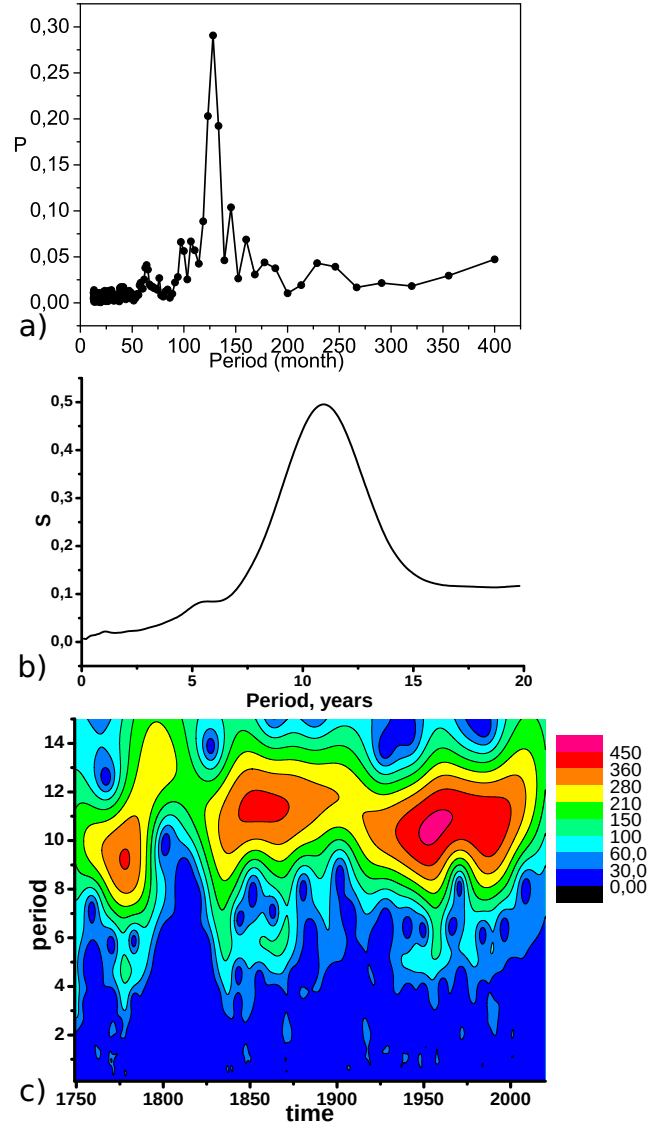


Figure 2. a) Fourier spectrum for the monthly mean sunspot data for time interval 1749 - 2019. P denotes the amplitudes of the Fourier harmonics normalized to the sum of their moduli. The harmonic of the maximal amplitude corresponds to the 25th harmonic, i.e., 126 months. The spectral resolution in the spectrum calculated is about five months. Panel b) shows integral wavelet spectra for sunspot data, and panel c) shows the wavelet plane for the real part of the modulus of the sunspot wavelet coefficients.

solar dynamo, while the solar equatorial dipole is something not obligatory for the solar activity cycle.

The QSO period varies from cycle to cycle both for the sunspot and the axial dipole data sets. The period of the axial dipole QSO changed from about 5 years near the minimum of cycles 21 and 22 to 6-7 years near the minimum of cycle 23 (i.e., approximately in 2004 and 2010). Also, we see that the maxima of the axial dipole QSO are approximately located at the ascending and descending branches of the axial dipole cycle.

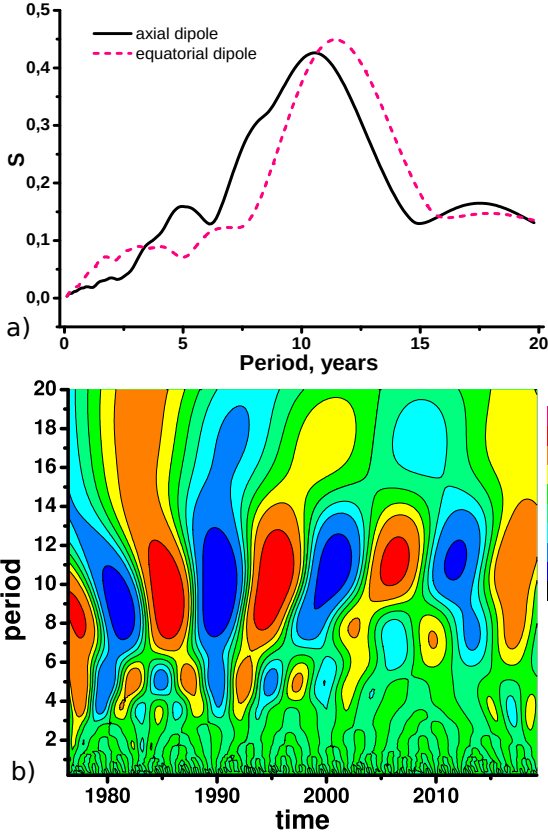


Figure 3. a) Integral wavelet spectra for the solar axial dipole data; b) wavelet plane for the real part of the modulus of the axial dipole wavelet coefficients.

6 RESULTS: QSO IN THE SIMULATIONS FROM OUR DYNAMO MODEL

Now, compare the results of the spectral analysis based on observational data with the data derived from the mean-field dynamo model. A preliminary analysis shows that QSO variations in the axial dipole can be reproduced in terms of different mean-field dynamo models, e.g., the 1D models proposed by Moss et al. (2008) and the recent 2D model proposed by Pipin & Kosovichev (2020). We have found out that the presence of the non-linear dynamo saturation effect is sufficient for the emergence of QSO both in the parameters of the toroidal magnetic field and in the axial dipole.

For our study, we need the parameters of both the axisymmetric and non-axisymmetric large-scale magnetic fields. For this reason, we use the simplified version of the non-axisymmetric dynamo model. The model simulates the dynamo process in a thin layer deep within the convection zone. The effect of magnetic buoyancy seeds the bipolar active region at a random position within the large-scale toroidal magnetic field. This effect accounts for the escape of magnetic energy from the dynamo region, as well. Following Frick et al. (2020), we use the mean density of the axisymmetric toroidal magnetic field as a proxy for sunspot activity:

$$\overline{B_\phi} = \frac{1}{2} \int_{-1}^1 |B_\phi| d\mu, \quad (18)$$

where $\mu = \cos \theta$ (θ is the polar angle), and the total unsigned

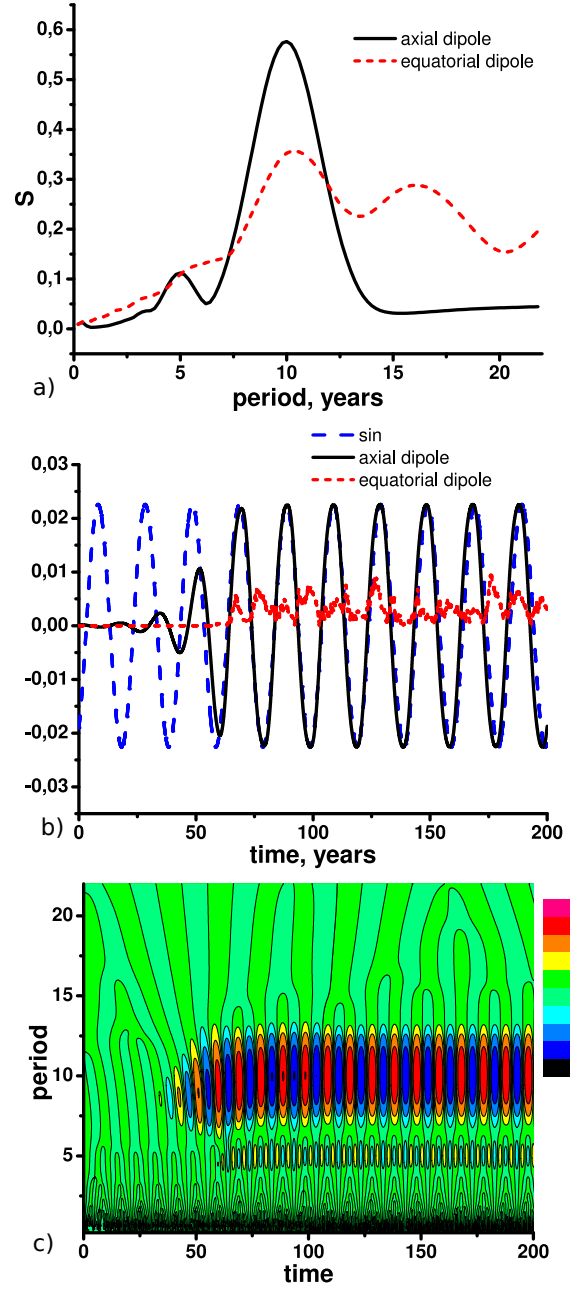


Figure 4. Dynamo model, upper panel: a - the integral wavelet spectra for the axial and equatorial dipole, b - the time evolution of the axial dipole (black line). The red line shows the absolute value of the equatorial dipole, and the blue line shows the sinus signal; c - the wavelet plane for the real part of the wavelet coefficients for the axial dipole.

flux of the radial magnetic field is

$$F_S = \int |B_r| dS, \quad (19)$$

where the integration is performed over the visible hemisphere. Frick et al. (2020) used F_S as a tracer of the sunspot activity to study QBO.

The integral wavelet spectrum (Fig.4, upper panel) for the absolute value of the axial dipole does contain a 5-year peak. The 11-year peak is present, as well. The equatorial dipole does not show this variation.

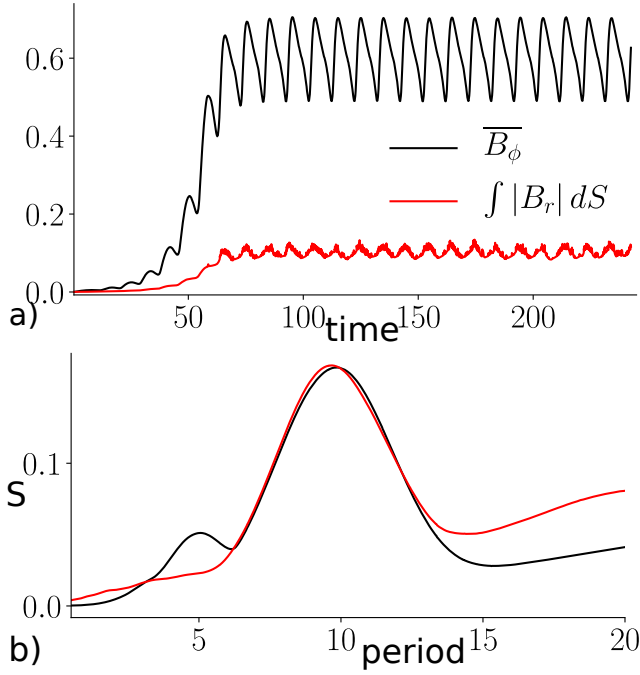


Figure 5. a) Evolution of the mean flux density of the toroidal magnetic field (black line) and the total flux density of the radial magnetic field (red line); both are shown in dimensionless units; b) their integral wavelet spectra.

To clarify the nature of the QSO periodicity, we have followed the evolution of the magnetic field starting with the tiny seed magnetic field (Fig. 4, middle panel). It is found out that the 11-year periodicity starts at the very beginning of the magnetic field evolution. Quasi-sexennial oscillations gain considerable power, when the dynamo cycle becomes stationary as the magnetic energy reaches the nonlinear saturation state. This means that the QSO can be considered a nonlinear effect. Note that the nonlinear saturation in the model is due to the magnetic buoyancy effect. The middle panel in Fig. 4 shows the time evolution of the axial and equatorial dipoles. The latter looks like noise, while the time evolution of the axial dipole seems to be almost sinusoidal. Also, we have found out that the maximum power of the axial dipole QSO is observed at the rise and decline of the axial dipole cycle. This dynamo-model result agrees qualitatively with our observational findings.

Figure 5 shows the evolution and wavelet spectra for the mean flux density of the toroidal magnetic field, \overline{B}_ϕ , the total flux density of the radial magnetic field, F_S , and their integral wavelet spectra. The nonlinear phase of the evolution of \overline{B}_ϕ is strictly periodic. However, the shape of the \overline{B}_ϕ signal differs strongly from the sine signal. Similar to the axial dipole, the integral spectrum of \overline{B}_ϕ clearly shows QSO with a period of 5 years (half a dynamo cycle). We do not show the wavelet plane of \overline{B}_ϕ . It is qualitatively very similar to that of the axial dipole with the maximum QSO power in the rise and decline phases of the \overline{B}_ϕ cycle.

To separate the QSO from the main magnetic cycle, we subtract the pure sinusoidal signal from the signal of the axial dipole. For the toroidal magnetic field, we subtract the absolute value of the sinusoidal signal. The results are shown in Fig. 6. The resulting signal shows tiny 5-year

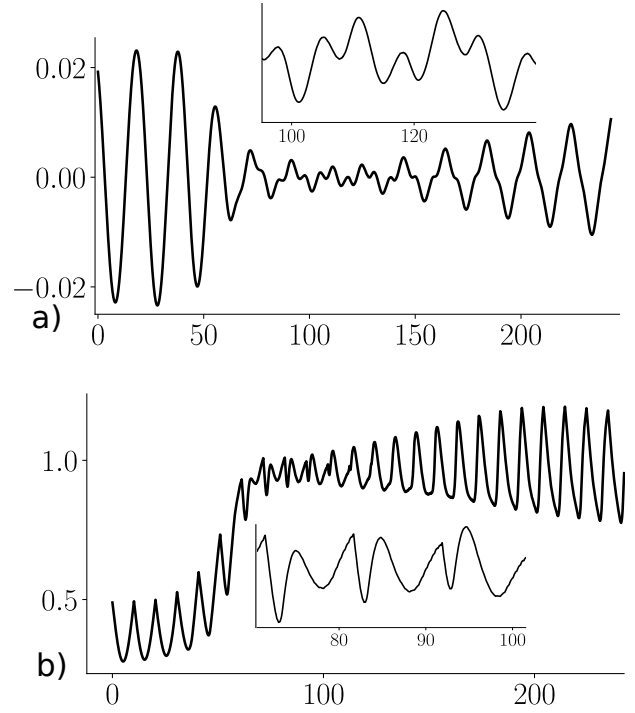


Figure 6. The sinus signal subtracted from the axial dipole: a) magnetic dipole time series, b) the same for the toroidal magnetic field. The small plots on the right present the most instructive parts of the plots.

variations when the phase of the axial dipole and the sine are synchronized (Fig. 6, top). The oscillation magnitude is rather small compared to the main signal. We have enlarged the piece of the trajectory containing a clear 5-year oscillation and have superimposed it on the main panel. The \overline{B}_ϕ parameter shows a qualitatively similar result. However, the cycle of the toroidal magnetic field deviates strongly from a sine curve. Therefore, the extracted QSO differs very much from the regular oscillation.

In our model, the axisymmetric toroidal field of strength $|B_\phi| > 0.5$ produces bipolar regions. Evolution of the total flux of the radial magnetic field, F_S , from these bipolar regions is shown in Fig. 5 as well. We see that, in our model, only a small part of the flux of the toroidal magnetic field is transformed into magnetic bipolar regions. The integral wavelet of F_S does not show QSO (Fig. 5b). This does not mean that QSO in F_S are absent at all.

Figure 7 shows a piece of the F_S trajectory for the nonlinear stage of the dynamo evolution and its wavelet plane for this time interval. We see, that the shape of the F_S cycle differs from the cycle of \overline{B}_ϕ . The F_S spectrum contains variations in the range of periods of both QBO and QSO. However, these intervals seem to have no gap in between. Therefore the QSO power is not pronounced in the integral spectrum. It is interesting to note that, in the given time interval, the greatest power of QSO with a 5-year period was observed near the minima of the F_S trajectory. This differs from the behavior of \overline{B}_ϕ .

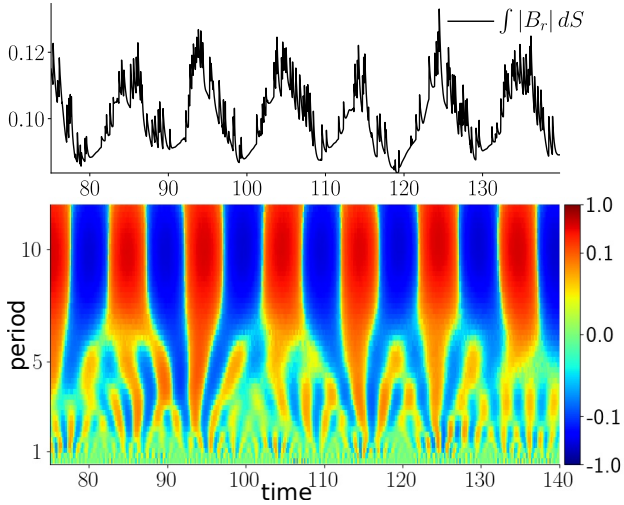


Figure 7. a) Evolution of the total flux of the radial magnetic field, F_S ; b) wavelet plane for the real part of wavelet coefficients of F_S .

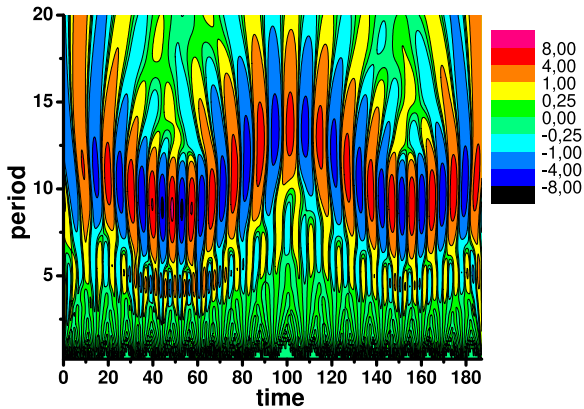


Figure 8. 2D wavelet spectra for the model with a variable α effect.

7 DISCUSSION AND CONCLUSIONS

We have isolated QSO hidden in the phenomenon of solar activity using sunspot data and the record of solar magnetic dipole. These time series trace the magnetic field components involved in the solar dynamo, which maintains the main solar cycle, i.e., the toroidal and poloidal components. We have reproduced a very similar behavior using a relatively simple solar dynamo model, which is, however, sophisticated enough to include the non-axisymmetric solar magnetic field. We have uncovered that in our model, the axial dipole and the mean density of the toroidal magnetic field display QSO only during the nonlinear stage of the dynamo evolution. As directly follows from the analysis, the axial-dipole QSO can be interpreted as variations in the shape of the axial dipole cycle due to the non-linearity of the underlying dynamo process. In our model, the main non-linearity comes from the magnetic buoyancy effect. This effect results in a strongly asymmetric shape of the toroidal magnetic field cycle. In the model, the poloidal magnetic field is produced from the toroidal field by the α effect. The shape of the dipole cycle becomes asymmetric because of the asymmet-

ric shape of the $\overline{B_\phi}$ cycle. Therefore, the axial-dipole QSO is inherent to the QSO of $\overline{B_\phi}$. The toroidal magnetic field in our model, besides participating in the dynamo process, produces bipolar regions. These bipolar regions modulate the total flux of the radial magnetic field on the surface, F_S . This parameter does not show QSO in the integral wavelet. This may be due to nonlinear multi-scale B^2 processes in the evolution of the non-axisymmetric magnetic fields that are initiated by the formation of bipolar regions. It is noteworthy that the QSO in sunspots are less pronounced than the axial-dipole QSO. This empirical result may be related to the QSO saturation effect similar to that found for the F_S parameter.

Another possible explanation is that the sunspot data series are much longer than those for the axial dipole. Note that observations show long-term variation in the QSO parameters. A weak axial-dipole cycle tends to have a longer QSO period. For example, the period of the axial-dipole QSO was shorter in cycles 21 and 22 than in cycles 23 and 24 (see, Fig.3). This conclusion is not robust because we have actual observational data for only a few cycles. We find that the given conclusion can be drawn using the time series from dynamo simulations that show a long-term variability. We checked it using the time series in the recent model by Pipin & Kosovichev (2020) (i.e., model C4). Note that in this model, the long-term variation of the magnetic activity was derived from *regular* centennial variations of the α effect (for more details see the paper cited above). Variations in the period of the axial dipole cycle and QSO variations in that dynamo model outputs are shown in Figure 8. We see that the shift of the cycle period results in the corresponding shift of the QSO period. This is in qualitative agreement with the results shown in Fig. 2c earlier. The model shows the period of the dipole cycle to increase to about 15 years during the grand minimum. The corresponding QSO almost disappear during this period. The model shows a similar behavior of the long-term evolution of QSO of the mean flux density of the toroidal magnetic field. It is noteworthy that the integral of the wavelet spectrum shown in Fig.3 shows no considerable power in the QSO range because of dispersion. Bearing in mind our mechanism of QSO, we suggest that the analysis of longer observational time-series of the axial dipole may reveal saturation of the QSO power in the case of strong variations in the axial dipole cycle.

We admit that other origins for a given QSO can exist as well. For example, in the flux-transport models the evolution of the axial dipole parameters can depend on variations in the meridional circulation. This mechanism should be studied separately. Note, that the model by Pipin & Kosovichev (2020) is the state of the art non-kinematic mean-field axisymmetric dynamo model. The results concerning the QSO derived from this model need further investigation. We mention them here to support our primary conclusion that the non-linear dynamo effects are the main source of QSO. A QSO has half the period (twice the frequency) of the basic cycle; so the form of nonlinearity must ensure this. The magnetic buoyancy is the $|B|^2$ effect. Also, we have analyzed how different kinds of the α -effect nonlinearities affect the QSO. For example, we have studied dynamo models with the so-called "algebraic" and dynamic α - effect nonlinearity. The latter results from the magnetic helicity conservation. We find that these nonlinearities result in anharmonic shapes

of the toroidal magnetic field cycles. Similarly to the magnetic buoyancy, these nonlinear dynamo effects have the $|B|^2$ - type dependence on the strength of the large-scale magnetic field. Therefore, they can result in modulating the α effect, as well as in the escape of magnetic field with the doubling of frequency relative to the original frequency of the mean magnetic field strength. This causes anharmonic shapes of the toroidal magnetic field cycles (see, [Baliunas et al. \(2006\)](#)), and it makes the QSO features robust for the stationary phase of the dynamo evolution in our models.

We note, however, that some other parameters are not robust. For example, the 11-year cycle in the equatorial dipole is not well seen in the models with the "algebraic", B^{-2} , non-linearity of the α - effect. The above discussion does not exclude that some QSO power can stem from random fluctuation in the shape of the activity cycles. To distinguish between the random and regular mechanisms generating the QSO, we need to extend our study. This can be done using more sophisticated data mining tools and dynamo models with random fluctuations.

A related point is that nonlinear dynamos are often invoked to explain lower frequencies in the records of solar activity (i.e., modulation of the basic cycle on longer timescales). This approach is a natural consequence of nonlinear interactions between the basic parity modes of the dynamo-generated magnetic field (see [Ivanova & Ruzmaikin 1976](#); [Brandenburg et al. 1989](#); [Sokoloff & Nesme-Ribes 1994](#); [Knobloch et al. 1998](#); [Weiss & Tobias 2016](#)). It was found that if two different parity modes (e.g., symmetric and antisymmetric about the equator) have both close dynamo periods and dynamo excitation thresholds, then their nonlinear interactions can result in the modulation of the total magnetic energy with a long period determined by the difference between the mode frequencies. Also, the nonlinear interaction of a large-scale magnetic field and large-scale flows can result in modulation of the magnetic activity (see, [Brandenburg et al. 1991](#); [Knobloch et al. 1998](#); [Pipin 1999](#); [Küker et al. 1999](#)). In both cases, the time scale of the parity mode interactions and the relaxation of magnetic perturbations affect the large-scale flows over time intervals longer than the main dynamo period. This is opposite to the effects of the magnetic cycle shape variations discussed in this paper. Certainly, it is a very attractive and challenging task to study the nonlinear dynamo mechanisms on short and long time scales as part of the continuous transport of the magnetic and kinetic energy in the system. It looks plausible that these phenomena should be presented in various nonlinear systems, and their further investigation seems to be promising.

To sum up, we can draw the following conclusions. Observations show the existence of QSO both in the sunspot number record and in the proxies of the global magnetic field of the Sun, e.g., the evolution of the solar axial dipole. The dynamo models show that these QSO result from the nonlinear, anharmonic shape of the dynamo cycle. The inter-scale dynamics initiated by the sunspot formation at the solar surface and the long-term dynamo variations result in long-term variations of QSO. This work opens a new window for future study.

Acknowledgements

The authors are grateful to the WSO teams for a free access to their data. The work was supported by RFBR

grants No. 20-02-00150, 18-02-00085 and 19-52-53045. VVP did the dynamo simulations as part of the scientific project FR II.16 of ISTP SB RAS.

We are also grateful to Dr. W.Sun (Harvard-Smithsonian Center for Astrophysics) for critical reading of the manuscript.

Data Availability Statements.

The observational data underlying this article are available at <http://wso.stanford.edu/> and <http://sidc.oma.be/silso/datafiles>

The python code of the dynamo model and its results are available at zenodo.org [Pipin \(2020\)](#).

REFERENCES

- Baliunas S., Frick P., Moss D., Popova E., Sokoloff D., Soon W., 2006, *MNRAS*, **365**, 181
- Bazilevskaya G., Broomhall A. M., Elsworth Y., Nakariakov V. M., 2014, *Space Sci. Rev.*, **186**, 359
- Brandenburg A., Krause F., Meinel R., Moss D., Tuominen I., 1989, *A&A*, **213**, 411
- Brandenburg A., Moss D., Rüdiger G., Tuominen I., 1991, *Geophysical & Astrophysical Fluid Dynamics*, **61**, 179
- Deng L. H., Li B., Xiang Y. Y., Dun G. T., 2014, *Advances in Space Research*, **54**, 125
- Deng L. H., Zhang X. J., Deng H., Mei Y., Wang F., 2020, *MNRAS*, **491**, 848
- Frick P., Sokoloff D., Stepanov R., Pipin V., Usoskin I., 2020, *MNRAS*, **491**, 5572
- Hoeksema J. T., 1991, in BAAS. pp 679–683
- Hoeksema J. T., Scherrer P. H., 1986, WDC Report UAG-94, NGDC, Boulder, CO
- Ivanova T. S., Ruzmaikin A. A., 1976, *Soviet Ast.*, **20**, 227
- Kitchatinov L. L., Pipin V. V., 1993, *A&A*, **274**, 647
- Knobloch E., Tobias S. M., Weiss N. O., 1998, *MNRAS*, **297**, 1123
- Krause F., Rädler K.-H., 1980, *Mean-Field Magnetohydrodynamics and Dynamo Theory*. Berlin: Akademie-Verlag
- Küker M., Arlt R., Rüdiger G., 1999, *A&A*, **343**, 977
- Livshits I. M., Obridko V. N., 2006, *Astronomy Reports*, **50**, 926
- Lou Y.-Q., Wang Y.-M., Fan Z., Wang S., Wang J. X., 2003, *MNRAS*, **345**, 809
- Moss D., Sokoloff D., Usoskin I., Tutubalin V., 2008, *Solar Phys.*, **250**, 221
- Parker E., 1955, *Astrophys. J.*, **122**, 293
- Pipin V. V., 1999, *A&A*, **346**, 295
- Pipin V., 2020, 2DSPDy-0.3, [doi:10.5281/zenodo.3928932](https://doi.org/10.5281/zenodo.3928932)
- Pipin V. V., Kosovichev A. G., 2018a, preprint, [p. arXiv:1808.05332](https://arxiv.org/abs/1808.05332) ([arXiv:1808.05332](https://arxiv.org/abs/1808.05332))
- Pipin V. V., Kosovichev A. G., 2018b, *ApJ*, **867**, 145
- Pipin V. V., Kosovichev A. G., 2020, arXiv e-prints, [p. arXiv:2004.08537](https://arxiv.org/abs/2004.08537)
- Prabhakaran Nayar S. R., Radhika V. N., Revathy K., Ramadas V., 2002, *Sol. Phys.*, **208**, 359
- Rivin Y. R., Obridko V. N., 1992, *Azh*, **69**, 1083
- Scherrer P. H., Wilcox J. M., Svalgaard L., Duvall Jr. T. L., Dittmer P. H., Gustafson E. K., 1977, *Sol. Phys.*, **54**, 353
- Sokoloff D., Nesme-Ribes E., 1994, *A&A*, **288**, 293
- Weiss N. O., Tobias S. M., 2016, *MNRAS*, **456**, 2654